Large magnitude of the carbon isotope excursion during the Paleocene-Eocene Thermal Maximum

Qinghai Zhang[1,2*], Lin Ding[1], D. Clay Kelly[3], Kouki Kitajima[3,4], John W. Valley[3,4], Bo Zhang[5], Xiaoxia Xu[2], Helmut Willems[2,6], Andreas Klügel[2]

[1]Key Laboratory of Continental Collision and Plateau Uplift, Institute of Tibetan Plateau Research, Chinese Academy of Sciences, and CAS Center for Excellence in Tibetan Plateau Earth Sciences, Beijing 100101, China
[2]Department of Geosciences, University of Bremen, Bremen 28359, Germany
[3]Department of Geoscience, University of Wisconsin, Madison, WI 53706, USA
[4]WiscSIMS, Department of Geoscience, University of Wisconsin, Madison, WI 53706, USA
[5]The Key Laboratory of Orogenic Belts and Crustal Evolution, School of Earth and Space Sciences, Peking University, Beijing 100871, China
[6]Nanjing Institute of Geology and Palaeontology, Chinese Academy of Sciences, Nanjing 210008, China.

*E-mail: zhang@itpcas.ac.cn

Aug. 30, 2018
Final Publication:
Zhang Q, Ding L, Kitajima K, Valley JW, Zhang B, Xu X, Willems H, Kluegel A (2020) Large Magnitude of the Carbon Isotope Excursion During the Paleocene-Eocene Thermal Maximum. Global and Planetary Change. 184: 13 p. https://doi.org/10.1016/j.gloplacha.2019.103049

The Paleocene-Eocene thermal maximum (PETM) was an extraordinary pulse of global warming approximately 56 Ma. This warming event is associated with an addition of large amounts of ^{13}C-depleted carbon into the atmosphere-ocean system, but the magnitude of the negative carbon isotope excursion (CIE) signaling the PETM and often used to estimate mass of the released carbon is still debated. Here we gauge the CIE magnitude using secondary ion mass spectrometry (SIMS) to perform *in situ* $\delta^{13}C$ measurements within individual larger benthic foraminifera preserved in a tropical shallow marine limestone section in south Tibet. This SIMS-based $\delta^{13}C$ record yields a negative CIE (Δ~7‰) comparable in magnitude to that registered by terrestrial records but larger than the ~4‰ CIE returned by surface-dwelling planktonic foraminifera in deep-sea records. We therefore posit that the CIE magnitude was ~7‰ in the surface ocean, and that the previous ~4‰ estimates for the CIE are attenuated by incomplete preservation and diagenetic overprinting. The large CIE magnitude in the surface ocean (~7‰) and the evidently smaller CIE magnitude registered by deep-sea

benthic foraminifera (~2-3.5‰) are likely a function of rate and duration of carbon release as well as ocean stratification during the PETM.

The Paleocene-Eocene thermal maximum (PETM) was a geologically rapid global warming event that happened ~56 Ma ago and lasted ~200 kyr[1,2]. This event was associated with a perturbation to the global carbon cycle as evidenced by a sharp decrease in the carbon isotope compositions ($\delta^{13}C$) of both inorganic and organic carbon in exogenic carbon pools[3]. It is widely accepted that thousands of petagrams (Pg) of ^{13}C-depleted carbon was added into the atmosphere-ocean system during the PETM[4,5], which either triggered the initial warming or intensified the warming as a positive feedback[5-7]. The addition of ^{13}C-depleted carbon caused a ~6-8‰ decrease in the $\delta^{13}C$ of paleosol carbonate, enamel apatite, higher plant *n*-alkanes on land and bulk carbonate in shallow marine environments[8-15]. In contrast, the $\delta^{13}C$ decrease in the open ocean is estimated at ~4‰ for mixed-layer planktonic foraminifera[1,16] and ~2-3.5‰ for thermocline-dwelling planktonic foraminifera and small benthic foraminifera[1,17,18]. The term "carbon isotope excursion" (CIE) was coined to describe this $\delta^{13}C$ decrease, and the full CIE magnitude and its remarkable difference from different depositional environments are the subject of much debate[3,12,15,16,19-21].

It has been argued that the smaller CIE magnitude returned by pelagic sites might result from incomplete preservation stemming from carbonate dissolution fueled by carbon input during the PETM[12,22]. The lower part of the CIE stratigraphy in many pelagic PETM sections is marked by clay-rich calcareous ooze associated with an increased fragmentation of planktonic foraminifer shells[23] or claystone devoid of sedimentary calcite with a sharp basal contact[22]. For instance, the PETM section of Ocean Drilling Program (ODP) Site 690 contains one of the most complete CIE records recovered from deep-sea sedimentary archives to date, yet it has been estimated that as much as ~60% of sedimentary calcite has been lost to dissolution across the CIE onset in this reference section[24]. Given that the abundance of foraminifera in bulk sediment at Site 690 is low (~1-6%)[25] and planktonic foraminifera are more susceptible to dissolution than coccoliths[26], it is very likely that the foraminifer record at Site 690 is incomplete. To complicate matters, deep-sea benthic foraminifera experienced a major taxonomic turnover during the PETM with ~30-50 species succumbing to extinction[18]. Thus, if one assumes that peak pCO_2 concentrations scale with the severity of carbonate under-saturation and are signaled by the lowest $\delta^{13}C$ values, then it stands to reason that foraminifera recording the most negative $\delta^{13}C$ values of the CIE were dissolved and that deep-sea records might underestimate the true magnitude of the CIE.

Stratigraphic records of the CIE from terrestrial and shallow marine environments tend to be relatively expanded and not affected by carbonate dissolution. This does not imply, however, that the complete CIE event is preserved in these records. In these

environments, physical erosion or non-deposition frequently occurs and can leave numerous sedimentary hiatuses that may go unrecognized. A voluminous compilation of accumulation rates reveals that net accumulation rates decrease systematically as time spans increase (Fig. 1). This relationship was interpreted as reflecting the incomplete nature of sedimentary records[27,28], a phenomenon coined "Sadler effect"[29]. Thus, as time spans increase, many longer hiatuses are incorporated into the calculation of accumulation rates so that the rates will decrease. As time resolution increases and time spans decrease, some longer hiatuses are revealed, and calculated accumulation rates will increase by avoiding temporal gaps represented by these hiatuses[28]. In Sadler's compilation, accumulation rates in terrestrial and shallow marine environments decrease rapidly as time spans increase from 1 kyr to 100 kyr, which are relevant to the duration of the PETM-CIE (Fig. 1). This suggests that most terrestrial and shallow marine CIE records are, at least statistically, also incomplete. Therefore, the observed large CIE magnitude from terrestrial and shallow marine records should be viewed as a conservative estimate of the CIE magnitude, instead of the full CIE magnitude.

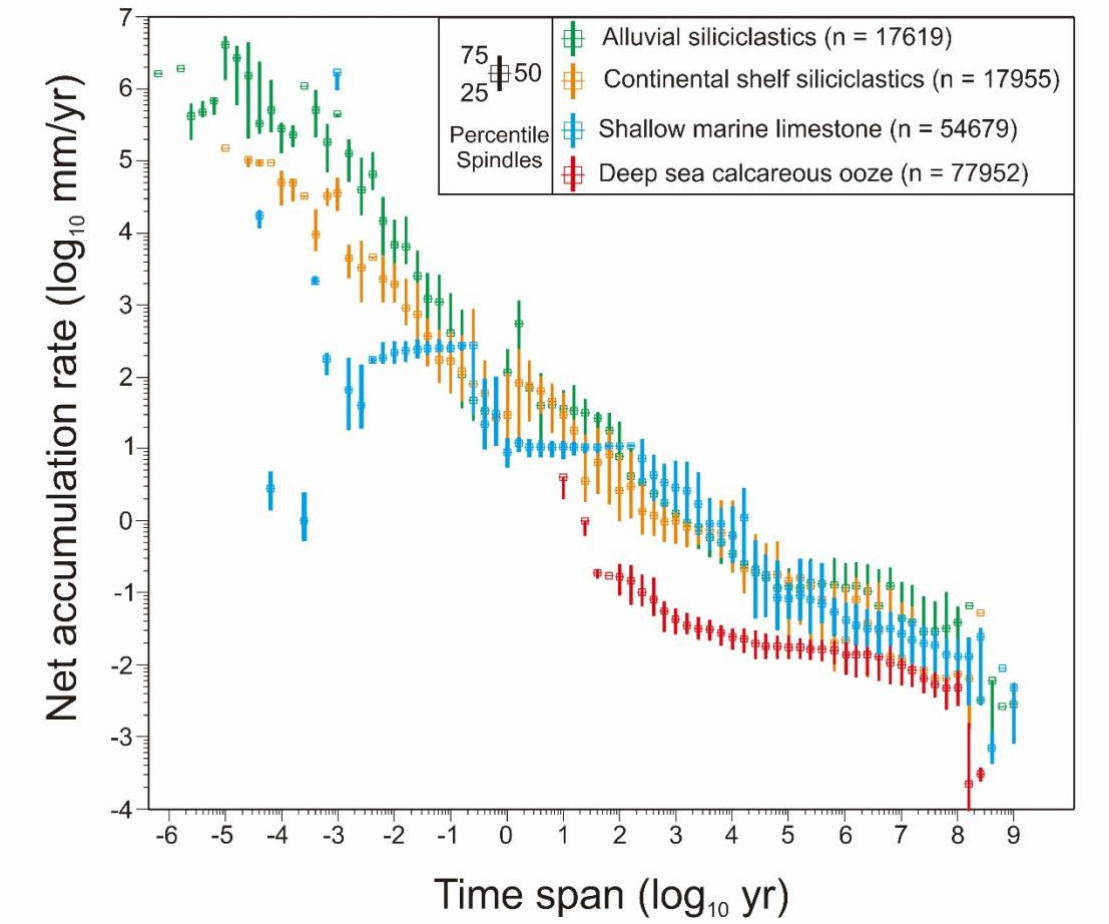

Fig. 1 A compilation of published accumulation rates of sediments in different depositional environments showing power law relationships between net accumulation rates and time spans. Distributions of median, 25th, 75th percentile values are determined for five time-span units per logarithm cycle with no smoothing or overlap (figure courtesy Peter Sadler).

Although it remains challenging to determine the true completeness of CIE records, some studies suggest that the stepped CIE preserved in bulk carbonate likely represents a more complete record of carbon perturbation during the PETM[15,22,30-33]. Several lines of evidence support the fidelity of the stepped CIE records in bulk carbonate: (1) In pelagic PETM sections, the major component in bulk carbonate is calcareous nannofossils (i.e., coccoliths)[25], and coccoliths have been shown to be more dissolution-resistant than foraminifera on the sea floor[26]. (2) Some culture experiments suggest that high CO_2 partial pressures can increase the calcification and net primary production in coccolithophores[34]. Collectively, bulk carbonate records from pelagic PETM sections should suffer less "time loss" than foraminifer records. (3) Inter-species vital effects in coccolith $\delta^{13}C$ during periods of relatively high pCO_2 concentrations (>375-575 ppm) were believed to be suppressed[35,36]. Specifically, inter-specific vital effects of coccolith $\delta^{13}C$ at ODP Site 690 was confirmed to be very small during the PETM[32]. (4) The stepped CIE is unlikely an artifact of bioturbation because it also appears in the section at Mead Stream (New Zealand) where no strong bioturbation was observed[31]. (5) The stepped structure of the CIE has been used to correlate PETM sections from geographically distant areas (Fig. 2)[15,30]. These sections were formed in different depositional environments and are presumably among the best preserved PETM sections in these depositional settings.

Here we constrain the CIE magnitude during the PETM based on a tropical, shallow marine carbonate section (13ZS) at Tingri (south Tibet) (Fig. 2). Most of the samples in section 13ZS contain ~95% carbonate[15] and are rich in larger benthic foraminifera that usually dwell in shallow-marine oligotrophic environments, implying insignificant continental river runoff in this area. Thus, section 13ZS has an advantage over sections formed in shallow-marine siliciclastic environments in that the PETM-CIE record in the former is not strongly complicated by river discharge, potentially preserving an "uncontaminated" marine CIE signal. In this study, we conduct *in situ* $\delta^{13}C$ measurements on shells of larger benthic foraminifera (LBF, >1 mm in diameter) by using secondary ion mass spectrometry (SIMS) (Supplementary Figs. 1-2). To assess possible diagenetic effects on the preservation of LBF shells, we use scanning electron microscopy-electron backscatter diffraction (SEM-EBSD) to analyze the crystallographic orientation of calcite grains forming LBF shells (Supplementary Fig. 3) and laser ablation inductively coupled plasma mass spectrometry (LA-ICPMS) to measure *in situ* Mn/Ca, Y/Ca, La/Ca, and Ce/Ca ratios from the LBF shells (Fig. 3). These new data provide a better constraint on the true CIE magnitude in the surface ocean and shed a new light on the mass and fate of carbon taken up by the ocean during the PETM.

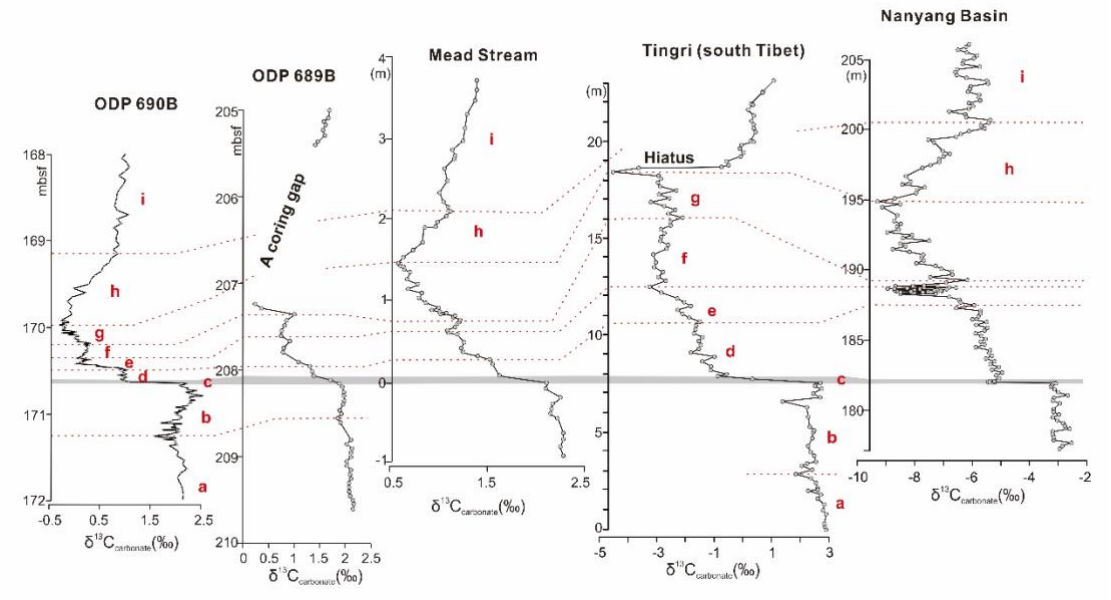

Fig. 2 Correlation of the stepped CIE among pelagic/hemipelagic sections (ODP Sites 690B & 689B, and Mead Stream in New Zealand), a shallow-marine carbonate section (13ZS section at Tingri, south Tibet), and a lacustrine carbonate section (Yuhuangding section in the Nanyang Basin, China). Raw data are taken from refs [15,23,30,31,33].

Section, samples and methods

Studied samples are collected from section 13ZS that is exposed at Tingri in south Tibet[15]. During the PETM, Tingri was located on a shallow marine carbonate ramp at ~10° N paleolatitude within the Tethyan Himalaya and was at least ~300 km away from the southern shoreline of the Neo-Tethyan Ocean. Section 13ZS is ~22 m thick and comprises calcareous marl, marly nodular limestone, and nodular limestone, representing the upper nodular limestone of the Zhepure Shan Formation. The main CIE, herein defined as the interval positioned between the stratigraphic levels of the CIE onset at 7.6 m and the $\delta_{13}C$ minimum at 18.4 m, was delimited in section 13ZS by a previously published bulk-carbonate $\delta_{13}C$ record[15] (Fig. 3). A sedimentary hiatus and a sudden change in LBF assemblages occur at ~18.6 m of the section where the CIE recovery begins[15]. In section 13ZS, most of the samples are wackestone, packstone, and floatstone. The dominant components in the samples are micrites and LBF fragments, with minor clay and sparry calcite (Supplementary Fig. 1). Below ~18.6 m of the section, the LBF assemblages are composed of the genera *Lockhartia*, *Miscellanea*, *Operculina*, *Kathina*, and *Ranikothalia*, indicating a paleowater depth of ~40-80 m during the pre-CIE and main CIE time intervals[37].

Diagenesis

Previous study has demonstrated that limestone samples from section 13ZS have experienced water-rock interaction in a closed system that had an insignificant effect

on the $\delta_{13}C$ of measured bulk carbonate (i.e., micrites and LBF fragments)[15]. Here, we use EBSD data and Mn/Ca, Y/Ca, La/Ca, and Ce/Ca ratios to re-evaluate possible diagenetic effects on the $\delta_{13}C$ compositions of LBF shells.

The genera used in this study (*Miscellanea*, *Lockhartia* and *Operculina*) have hyaline, bilamellar, perforate walls that are made of low-Mg calcite. The calcite crystals have preferred orientation of the *c*-axes, normal to the wall surface and show the characteristic "radial microstructure"[38]. Strong diagenesis can alter the preferred crystallographic orientation of biogenic calcites and cause a variable degree of "crystallographic loss"[39]. Although recrystallization may occasionally alter chemical or isotopic compositions of foraminifer shells without affecting their crystal morphology, this usually happens if original foraminifer shells are made of chemically unstable aragonite or high-Mg calcite[40], not of low-Mg calcite. In section 13ZS, EBSD data obtained from pillars and chamber walls of *Miscellanea* show that their original crystallographic structure is still maintained (Supplementary Fig. 3), suggesting insignificant diagenesis in section 13ZS.

Some trace elements (Mn, Y, La, Ce) in foraminifer calcite can be used to evaluate diagenetic effects, among which Mn is the most reliable diagenetic proxy[41]. Generally, ratios of Mn/Ca, Y/Ca, La/Ca, and Ce/Ca in foraminifer calcite will increase as the degree of diagenetic alteration increases[41,42]. Modern *Operculina* specimens from neritic environments typically register characteristic Mn/Ca ratios of ~0.004-0.1 mmol/mol[42]. Some Eocene specimens of *Nummulites* and *Operculina* with glassy shells show higher Mn/Ca ratios of ~0.1-0.4 mmol/mol, and these specimens were suggested to have preserved primary shell chemistry[42]. We therefore consider Mn/Ca ratios <0.4 mmol/mol as indicating preservation of primary shell chemistry in fossilized LBF. In section 13ZS, the Mn/Ca ratios of LBF shells and micrites range from 0.05 mmol/mol to 0.3 mmol/mol, with most ratios being <0.2 mmol/mol. The difference in Mn/Ca ratios between co-occurring LBF shells and micrites is small (Fig. 3). The ratios of Y/Ca, La/Ca, and Ce/Ca cluster around ~6-12 μmol/mol, ~4-8 μmol/mol, and ~7-14 μmol/mol, respectively (Fig. 3). Although these ratios are ~10× higher than those from modern LBF specimens, they are very similar to those of Eocene-aged LBF having glassy shells[42]. We therefore conclude that diagenesis had a negligible effect on the preservation of primary geochemical signals in the LBF shells from section 13ZS.

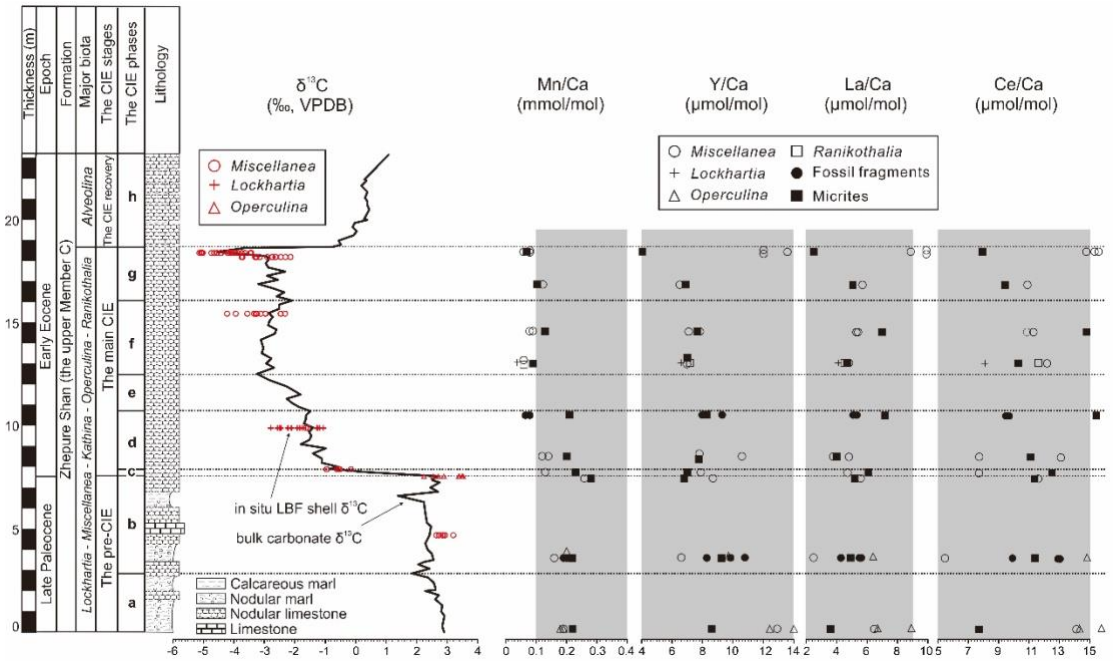

Fig. 3 Lithology, LBF assemblages, bulk carbonate $\delta_{13}C$ curve with *in situ* $\delta_{13}C$ from LBF shells (red symbols), and elemental ratios from section 13ZS. Dashed lines delimit different CIE phases, and grey shading highlights ranges of elemental ratios from Eocene-aged LBF with glassy shells[42]. Bulk carbonate $\delta_{13}C$ curve from ref [15].

The $\delta_{13}C$ of different carbonate components

In section 13ZS, we measured *in situ* $\delta_{13}C$ of different carbonate components from seven limestone samples. Two samples at 4.70 m and 7.55 m are located within the pre-CIE interval, and the rest are from the main CIE interval. The sample at 18.40 m documents the most negative $\delta_{13}C$ value during the PETM (Fig. 4).

In situ $\delta_{13}C$ measurements show that intra-shell $\delta_{13}C$ variability in shells of *Miscellanea* and *Lockhartia* is very limited (Figs. 4A & 4C) or slightly evident (Figs. 4D-4G), and that $\delta_{13}C$ values measured from these two genera are indistinguishable (Fig. 4D). In contrast, *Operculina* exhibits a systematic intra-shell $\delta_{13}C$ variation where $\delta_{13}C$ values of chamber walls and septa in the inner whorl are ~0.9‰ lower than those in the outer whorl (Fig. 4B). Micrite $\delta_{13}C$ roughly co-varies with LBF shell $\delta_{13}C$ (Figs. 4B, 4E & 4G), exhibiting a large decline in the main CIE interval (Figs. 4E & 4G). Except for the sample at 4.70 m, bulk carbonate $\delta_{13}C$ values in the remaining samples are very close to average $\delta_{13}C$ values of LBF shells from the same stratigraphic sample (Fig. 4).

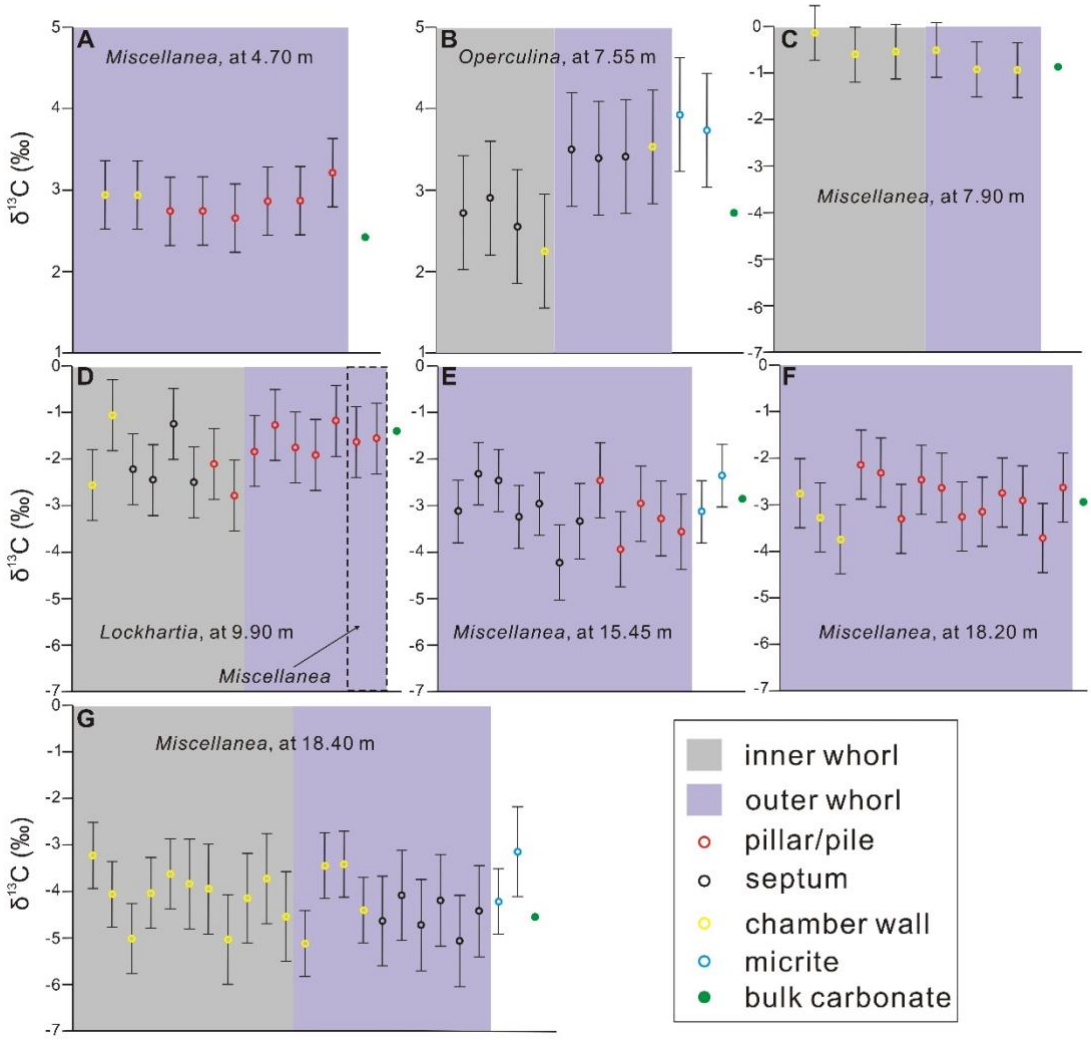

Fig. 4 Intra-shell $\delta_{13}C$ variability delineated by series of *in situ* SIMS analyses taken from pillar/pile, septum, chamber wall of LBF shells from pre-CIE (A-B) and main CIE (C-G) samples of section 13ZS. Correlative $\delta_{13}C$ values of micrite and bulk carbonate are also shown for comparison. The $\delta_{13}C$ values with error bars are obtained from *in situ* SIMS measurements (this study), and the $\delta_{13}C$ of bulk carbonate was measured using conventional isotope ratio mass spectrometry[15]. Note the CIE onset (phase **c** in the stepped CIE) is constrained by initial $\delta_{13}C$ decrease between ~7.55 m and ~7.90 m, and the main CIE terminates at ~18.40 m of section 13ZS. Error bars denote two standard deviations.

Although it remains unclear whether vital effects have influenced the $\delta_{13}C$ compositions of *Miscellanea* and *Lockhartia*, the limited intra-shell and inter-genus $\delta_{13}C$ variations registered by these two taxa suggest that the $\delta_{13}C$ of their shells are mainly controlled by the $\delta_{13}C$ of dissolved inorganic carbon in ambient seawater. With respect to *Operculina*, however, the increase in shell $\delta_{13}C$ values towards the outer whorl indicates that, in addition to the seawater $\delta_{13}C$, some physiological processes such as symbiont photosynthesis and respiration may have affected the shell $\delta_{13}C$ (ref [43]).

Micrites in shallow marine limestone have multiple sources; nevertheless, the $\delta_{13}C$

similarity between micrites and LBF indicates that micrites may result from physical or biological abrasion/disintegration of skeletal materials, such as LBF shells. Alternatively, micrites could be a result of cementation during early marine burial diagenesis[44]. In this case, cementation in section 13ZS should have been completed within ~1-2 kyr after the deposition of biogenic clasts so that the chemistry of diagenetic fluid is still modulated by contemporary seawater. The rapid completion of cementation can be inferred from the $\delta^{13}C$ data at ~7.55 m and at ~7.90 m. In section 13ZS, the large $\delta^{13}C$ decrease from ~7.55 m to ~7.90 m represents the CIE onset (phase **c** in the stepped CIE), and the duration of phase **c** was suggested to be ~1-2 kyr according to orbital age model at ODP Site 690 (ref [2]). Apparently, the micrite $\delta^{13}C$ from the sample at ~7.55 m was not affected by the subsequent large decrease in seawater $\delta^{13}C$ at ~7.90 m (Figs. 4B-C), indicating that cementation in the sample at ~7.55 m should have been completed prior to deposition of the sample at ~7.90 m. This inference is compatible with previous studies of carbonate-sediment lithification in modern shallow marine environments reporting that Holocene sediments were cemented within several tens of years, with average cement growth rates of ~8-10 cm/kyr[45]. Rapid cementation would decrease porosity and permeability in sediments quickly, thereby inhibiting further diagenesis and allowing cements to preserve the isotopic composition of contemporary seawater[45]. In section 13ZS, bulk carbonate mainly consists of micrites and LBF fragments and these two carbonate components have similar $\delta^{13}C$ values (Figs. 4B, 4E & 4G). We therefore attribute the similar $\delta^{13}C$ values returned by bulk carbonate and LBF shells from the same stratigraphic sample to rapid cementation.

The CIE magnitude in the ocean

In section 13ZS, the new SIMS data show that *Miscellanea* at 18.40 m records the most negative $\delta^{13}C$ value during the PETM (mean $\delta^{13}C$ = -4.3‰) and *Operculina* at 7.55 m registers a latest mean pre-CIE $\delta^{13}C$ value of 3.0‰. The difference in the SIMS $\delta^{13}C$ values between them averages ~7.3‰. Since it is still uncertain whether inter-genus $\delta^{13}C$ variability exists between *Miscellanea* and *Operculina*, we constrain the CIE magnitude using the SIMS $\delta^{13}C$ value of *Miscellanea* at 4.70 m and obtain an average CIE magnitude of ~7.2‰ (Supplementary Table 1). In the box and whisker plot generated by SIMS data (Fig. 5), the CIE magnitude is indicated to be ~7‰ or ~7.3‰. Thus, the CIE magnitude from foraminifer shells (~7-7.3‰) is very similar to the CIE magnitude from bulk carbonate in the same section (~7‰)[15] and highly congruent with the ~7-8‰ $\delta^{13}C$ decrease in paleoatmospheric CO_2 inferred from paleosol carbonate $\delta^{13}C$ records in the Bighorn Basin, Wyoming[8,9].

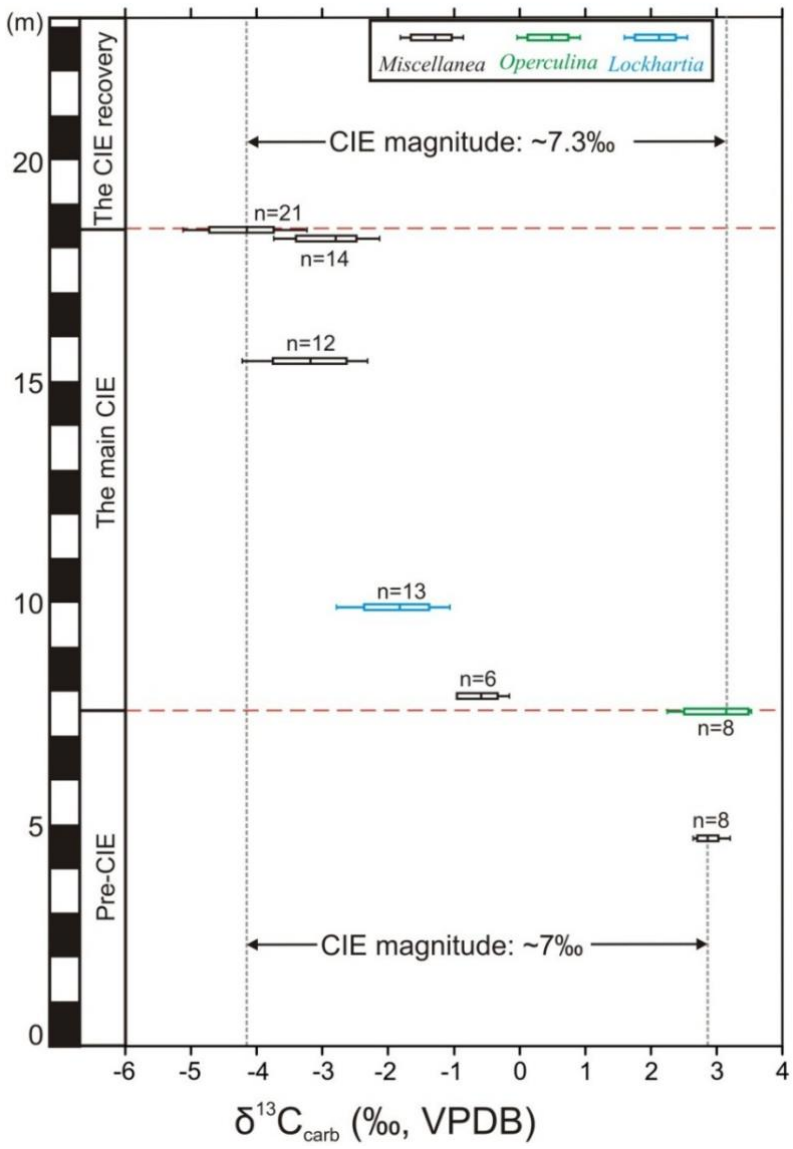

Fig. 5 Box and whisker plot illustrating the CIE magnitude registered by LBF shells from section 13ZS. Boxes represent the first and third quartiles of SIMS $\delta^{13}C$ values from analyzed LBF shells, and vertical lines within boxes denote the median values. Whiskers show the minimum and maximum $\delta^{13}C$ values. Two red dashed lines delimit the main CIE interval in section 13ZS.

During the PETM, a significant quantity of the ^{13}C-depleted carbon was released into the atmosphere[6,9]. Afterwards, the released carbon should have affected the surface ocean through air-sea CO_2 exchange and the deep ocean through ocean circulation. Mixing time for carbon exchange between atmosphere and surface ocean is decades[46], which is short enough for $\delta^{13}C$ in the atmosphere and surface ocean to equilibrate. Thus, both atmosphere and the surface ocean should record a similar CIE magnitude during the PETM. This inference is supported by some previous studies. In the Bighorn Basin, paleosol carbonate and enamel apatite records yielded a negative CIE magnitude of ~7-8‰ (refs [8,9]) and ~5.7-5.9‰ (refs [10,11]), respectively. Moreover, a CIE magnitude of ~6‰ was reported from paleosol carbonate in the Henyang Basin[47] and in the Tremp Basin[13], from higher plant *n*-alkanes in the Arctic[12], and from bulk

carbonate in the Nanyang Basin[33]. These CIE magnitude values are generally consistent with the CIE registered by LBF shells at Tingri, suggesting that the $\delta^{13}C$ in the atmosphere and surface ocean decreased by ~7‰ during the PETM. Regarding the smaller CIE magnitude (~4‰) registered by surface-dwelling planktonic foraminifera at ODP Site 690, we tentatively ascribe to a transient increase in carbonate dissolution that truncated pelagic PETM records rendering them incomplete[12,22] and/or diagenetic overprinting of foraminifer specimens[20].

For the entire ocean, however, time for the $\delta^{13}C$ equilibration between the surface ocean and the deep ocean was suggested to be multi-millennia[46,48]. Although the degree of ocean stratification and its effect on equilibration time are not precisely known, enhanced ocean stratification during the PETM[49] should have slowed down the rate of ocean circulation and prolonged the mixing time. Considering the relatively small carbon mass of the surface ocean (1,000 Pg) and the much larger carbon mass of the deep ocean (38,000 Pg), a prolonged equilibrium time may have resulted in a smaller $\delta^{13}C$ anomaly in the deep ocean. Recent modeling also suggests that the CIE magnitude in the surface ocean may differ markedly from that in the deep ocean, depending on the rate, duration, and mass of released ^{13}C-depleted carbon[50]. Indeed, the reported largest CIE magnitude from benthic foraminifera is ~3.5‰ at ODP Site 1263 (ref [17]), although this value may also be attenuated by carbonate dissolution and/or benthic foraminifer extinction.

Collectively, we suggest that both the atmosphere and the surface ocean should have had similar CIE magnitude (~7‰) during the PETM. However, the CIE magnitude in the deep ocean might be smaller, depending on rate and duration of light carbon release as well as the severity of ocean stratification. Our finding has implications for understanding the fate of the released light carbon during the PETM and calls for future modeling work to further characterize the detailed process of carbon propagation in the PETM ocean.

References

1. Kennett, J.P., Stott, L.D., 1991. Abrupt deep-sea warming, palaeoceanographic changes and benthic extinctions at the end of the Palaeocene. Nature 353, 225-229.
2. Röhl, U., Westerhold, T., Bralower, T.J., Zachos, J.C., 2007. On the duration of the Paleocene-Eocene thermal maximum (PETM). Geochemistry Geophysics Geosystems 8, doi:10.1029/2007GC001784.
3. McInerney, F.A., Wing, S.L., 2011. The Paleocene-Eocene Thermal Maximum: A perturbation of carbon cycle, climate, and biosphere with implications for the future. Annual Review of Earth and Planetary Sciences 39, 489-516.
4. Meissner, K.J., Bralower, T.J., Alexander, K., Jones, T.D., Sijp, W., Ward, M., 2014. The Paleocene-Eocene Thermal Maximum: How much carbon is enough? Paleoceanography 29, 946-963.

5. Dickens, G.R., O'Neil, J.R., Rea, D.K., Owen, R.M., 1995. Dissociation of oceanic methane hydrate as a cause of the carbon isotope excursion at the end of the Paleocene. Paleoceanography 10, 965-971.
6. Thomas, D.J., Zachos, J.C., Bralower, T.J., Thomas, E., Bohaty, S., 2002. Warming the fuel for the fire: Evidence for the thermal dissociation of methane hydrate during the Paleocene-Eocene thermal maximum. Geology 30, 1067-1070.
7. Zachos, J.C., Dickens, G.R., Zeebe, R.E., 2008. An early Cenozoic perspective on greenhouse warming and carbon-cycle dynamics. Nature 451, 279-283.
8. Bains, S., Norris, R.D., Corfield, R.M., Bowen, G.J., Gingerich, P.D., Koch, P.L., 2003. Marine-terrestrial linkages at the Paleocene-Eocene boundary. Geological Society of America Special Papers 369: 1-9.
9. Bowen, G.J., Koch, P.L., Gingerich, P.D., Norris, R.D., Bains, S., Corfield, R.M., 2001. Refined isotope stratigraphy across the continental Paleocene-Eocene boundary on Polecat Bench in the Northern Bighorn Basin, in: Gingerich, P.D. (Ed.), Paleocene-Eocene stratigraphy and biotic change in the Bighorn and Clarks Fork Basins, Wyoming. University of Michigan Papers on Paleontology, pp. 73-88.
10. Bowen, G.J., Maibauer, B.J., Kraus, M.J., Rohl, U., Westerhold, T., Steimke, A., Gingerich, P.D., Wing, S.L., Clyde, W.C., 2015. Two massive, rapid releases of carbon during the onset of the Palaeocene-Eocene thermal maximum. Nature Geoscience 8, 44-47.
11. Koch, P.L., Zachos, J.C., Gingerich, P.D., 1992. Correlation between isotope records in marine and continental carbon reservoirs near the Palaeocene/Eocene boundary. Nature 358, 319-322.
12. Pagani, M., Pedentchouk, N., Huber, M., Sluijs, A., Schouten, S., Brinkhuis, H., Sinninghe Damste, J.S., Dickens, G.R., Expedition Scientists, 2006. Arctic hydrology during global warming at the Palaeocene/Eocene thermal maximum. Nature 442, 671-675.
13. Schmitz, B., Pujalte, V., 2003. Sea-level, humidity, and land-erosion records across the initial Eocene thermal maximum from a continental-marine transect in northern Spain. Geology 31, 689-692.
14. Wright, J.D., Schaller, M.F., 2013. Evidence for a rapid release of carbon at the Paleocene-Eocene thermal maximum. Proceedings of the National Academy of Sciences 110, 15908-15913.
15. Zhang, Q., Wendler, I., Xu, X., Willems, H., Ding, L., 2017. Structure and magnitude of the carbon isotope excursion during the Paleocene-Eocene thermal maximum. Gondwana Research 46, 114-123.
16. Zachos, J.C., Bohaty, S.M., John, C.M., McCarren, H., Kelly, D.C., Nielsen, T., 2007. The Palaeocene–Eocene carbon isotope excursion: constraints from individual shell planktonic foraminifer records. Philosophical Transactions of the Royal Society A 365, 1829-1842.
17. McCarren, H., Thomas, E., Hasegawa, T., Röhl, U., Zachos, J.C., 2008. Depth dependency of the Paleocene-Eocene carbon isotope excursion: Paired benthic and terrestrial biomarker records (Ocean Drilling Program Leg 208, Walvis Ridge).

Geochemistry Geophysics Geosystems 9, doi:10.1029/2008GC002116.
18. Thomas, E., Shackleton, N.J., 1996. The Paleocene-Eocene benthic foraminiferal extinction and stable isotope anomalies, in: Knox, R.W.O.B., Corfield, R.M., Dunay, R.E. (Eds.), Correlation of the Early Paleogene in Northwest Europe. Geological Society London Special Publications, London, pp. 401-441.
19. Bowen, G.J., Beerling, D.J., Koch, P.L., Zachos, J.C., Quattlebaum, T., 2004. A humid climate state during the Palaeocene/Eocene thermal maximum. Nature 432, 495-499.
20. Kozdon, R., Kelly, D.C., Valley, J.W., 2018. Diagenetic attenuation of carbon isotope excursion recorded by planktic foraminifers during the Paleocene-Eocene thermal maximum. Paleoceanography and Paleoclimatology, doi:10.1002/2017PA003314.
21. Schubert, B.A., Jahren, A.H., 2013. Reconciliation of marine and terrestrial carbon isotope excursions based on changing atmospheric CO_2 levels. Nature Communications 4, 1-6.
22. Zachos, J.C., Rohl, U., Schellenberg, S.A., Sluijs, A., Hodell, D.A., Kelly, D.C., Thomas, E., Nicolo, M., Raffi, I., Lourens, L.J., McCarren, H., Kroon, D., 2005. Rapid acidification of the ocean during the Paleocene-Eocene thermal maximum. Science 308, 1611-1615.
23. Kelly, D.C., Nielsen, T.M.J., Schellenberg, S.A., 2012. Carbonate saturation dynamics during the Paleocene-Eocene thermal maximum: Bathyal constraints from ODP sites 689 and 690 in the Weddell Sea (South Atlantic). Marine Geology 303-306, 75-86.
24. Bralower, T.J., Kelly, D.C., Gibbs, S., Farley, K., Eccles, L., Lindemann, T.L., Smith, G.J., 2014. Impact of dissolution on the sedimentary record of the Paleocene-Eocene thermal maximum. Earth and Planetary Science Letters 401, 70-82.
25. Kelly, D.C., 2002. Response of Antarctic (ODP Site 690) planktonic foraminifera to the Paleocene–Eocene thermal maximum: Faunal evidence for ocean/climate change. Paleoceanography 17, doi:10.1029/2002PA000761.
26. Chiu, T.-C., Broecker, W.S., 2008. Toward better paleocarbonate ion reconstructions: New insights regarding the $CaCO_3$ size index. Paleoceanography 23, doi:10.1029/2008PA001599.
27. Sadler, P.M., 1981. Sediment accumulation rates and the completeness of stratigraphic sections. The Journal of Geology 89, 569-584.
28. Sadler, P.M., 1999. The influence of hiatuses on sediment accumulation rates. GeoResearch Forum 5, 15-40.
29. Schumer, R., Jerolmack, D.J.C.F.A., 2009. Real and apparent changes in sediment deposition rates through time. Journal of Geophysical Research 114, doi:10.1029/2009JF001266.
30. Bains, S., Corfield, R.M., Norris, R.D., 1999. Mechanisms of climate warming at the end of the Paleocene. Science 285, 724-727.
31. Nicolo, M.J., Dickens, G.R., Hollis, C.J., 2010. South Pacific intermediate water oxygen depletion at the onset of the Paleocene-Eocene thermal maximum as

depicted in New Zealand margin sections. Paleoceanography 25, doi:10.1029/2009PA001904.
32. Stoll, H.M., 2005. Limited range of interspecific vital effects in coccolith stable isotopic records during the Paleocene-Eocene thermal maximum. Paleoceanography 20, doi:10.1029/2004PA001046.
33. Zhu, M., Ding, Z., Wang, X., Chen, Z., Jiang, H., Dong, X., Ji, J., Tang, Z., Luo, P., 2010. High-resolution carbon isotope record for the Paleocene-Eocene thermal maximum from the Nanyang Basin, Central China. Chinese Science Bulletin 55, 3606-3611.
34. Iglesias-Rodriguez, M.D., Halloran, P.R., Rickaby, R.E.M., Hall, I.R., Colmenero-Hidalgo, E., Gittins, J.R., Green, D.R.H., Tyrrell, T., Gibbs, S.J., von Dassow, P., Rehm, E., Armbrust, E.V., Boessenkool, K.P., 2008. Phytoplankton calcification in a high-CO_2 world. Science 320, 336-340.
35. Bolton, C.T., Stoll, H.M., 2013. Late Miocene threshold response of marine algae to carbon dioxide limitation. Nature 500, 558-562.
36. Hermoso, M., Chan, I.Z.X., McClelland, H.L.O., Heureux, A.M.C., Rickaby, R.E.M., 2016. Vanishing coccolith vital effects with alleviated carbon limitation. Biogeosciences 13, 301-312.
37. Hottinger, L., 1997. Shallow benthic foraminiferal assemblages as signals for depth of their deposition and their limitations. Bulletin de la Société Géologique de France 168, 491-505.
38. Sen Gupta, B.K., 1999. Modern foraminifera. Kluwer Academic Publishers, Dordrecht.
39. Pérez-Huerta, A., Cusack, M., England, J., 2007. Crystallography and diagenesis in fossil craniid brachiopods. Palaeontology 50, 757-763.
40. Barrera, E., Huber, B.T., Savin, S.M., Webb, P.-N., 1987. Antarctic marine temperatures: Late Campanian through Early Paleocene. Paleoceanography 2, 21-47.
41. Lea, D., 1999. Trace elements in foraminiferal calcite, in: Sen Gupta, B.K. (Ed.), Modern Foraminifera. Kluwer Academic Publishers, pp. 259-277.
42. Evans, D., Müller, W., Oron, S., Renema, W., 2013. Eocene seasonality and seawater alkaline earth reconstruction using shallow-dwelling large benthic foraminifera. Earth and Planetary Science Letters 381, 104-115.
43. Spero, H.J., Lerche, I., Williams, D.F., 1991. Opening the carbon isotope "vital effect" black box, 2, Quantitative model for interpreting foraminiferal carbon isotope data. Paleoceanography 6, 639-655.
44. Munnecke, A., Westphal, H., Reijmer, J.J.G., Samtleben, C., 1997. Microspar development during early marine burial diagenesis: a comparison of Pliocene carbonates from the Bahamas with Silurian limestones from Gotland (Sweden). Sedimentology 44, 977-990.
45. Grammer, G.M., Ginsburg, R.N., Swart, P.K., McNeill, D.F., Jull, A.J.T., Prezbindowski, D.R., 1993. Rapid growth rates of syndepositional marine aragonite cements in steep marginal slope deposits, Bahamas and Belize. Journal of Sedimentary Petrology 63, 983-989.

46. Rohling, E.J., Sluijs, A., Dijkstra, H.A., Köhler, P., Wal, R.S.W.v.d., Heydt, A.S.v.d., Beerling, D.J., Berger, A., Bijl, P.K., Crucifix, M., DeConto, R., Drijfhout, S.S., Fedorov, A., Foster, G.L., Ganopolski, A., Hansen, J., Hönisch, B., Hooghiernstra, H., Huber, M., Huybers, P., Knutti, R., Lea, D.W., Lourens, L.J., Lunt, D., Masson-Demotte, V., Medina-Elizalde, M., Otto-Bliesner, B., Pagani, M., Pälike, H., Renssen, H., Royer, D.L., Siddall, M., Valdes, P., Zachos, J.C., Zeebe, R.E., 2012. Making sense of palaeoclimate sensitivity. Nature 491, 683-691.
47. Bowen, G.J., Clyde, W.C., Koch, P.L., Ting, S., Alroy, J., Tsubamoto, T., Wang, Y., Wang, Y., 2002. Mammalian dispersal at the Paleocene/Eocene boundary. Science 295, 2062-2065.
48. Wunsch, C., Heimbach, P., 2008. How long to oceanic tracer and proxy equilibrium? Quaternary Science Reviews 27, 637-651.
49. Winguth, A.M.E., Thomas, E., Winguth, C., 2012. Global decline in ocean ventilation, oxygenation, and productivity during the Paleocene-Eocene Thermal Maximum: Implications for the benthic extinction. Geology 40, 263-266.
50. Kirtland-Turner, S., Ridgwell, A., 2016. Development of a novel empirical framework for interpreting geological carbon isotope excursions, with implications for the rate of carbon injection across the PETM. Earth and Planetary Science Letters 435, 1-13.

Acknowledgements

We thank Peter Sadler for sharing his database, Anne Hübner and Patrick Monien for technical help in the laboratory. Funding for this research was provided by grants from the National Natural Science Foundation of China (41490615), National Key Research and Development Plan (2016YFC0600303), CAS Pioneer Hundred Talents Program, and the Deutsche Forschungsgemeinschaft (No. Wi725/29). WiscSIMS is supported by the U.S. National Science Foundation (EAR-1355590, 1658823) and the University of Wisconsin-Madison. John Valley is also funded by the U.S. Department of Energy (DE-FG02-93ER14389).

Author contributions

Q.Z., L.D., H.W., X.X. conceived the project, Q.Z. and X.X. carried out the field work, Q.Z., K.K. and J.W.V. conducted SIMS analysis, Q.Z. and B.Z. conducted EBSD analysis, Q.Z. and A.K. conducted LA-ICPMS analysis. All authors contributed to analyzing the data and the discussion. Q.Z. and D.C.K. wrote the manuscript.

Competing interests

The authors declare no competing interests.